Homogeneous nucleation of crystalline order in superdense liquid ^{4}He

F. Pederiva*
International School for Advanced Studies, via Beirut 2/4, 34014 Trieste, Italy

A. Ferrante
Fakultät für Physik, Universität Konstanz, Postfach 5560, D-78434 Konstanz, Germany

S. Fantoni
International School for Advanced Studies, via Beirut 2/4, 34014 Trieste, Italy
and International Centre for Theoretical Physics, Trieste, Italy

L. Reatto
Dipartimento di Fisica, Universitá degli Studi di Milano, via Celoria 16, Milano, Italy
(Received 23 February 1995)

We present the results of a numerical crystallization experiment in ^{4}He performed with the shadow wave function and the variational Monte Carlo method. The experiment consists in Monte Carlo simulations starting from liquidlike configurations of the atoms at a density well above the melting point. The system presents spontaneous nucleation of crystalline seeds, proving the spontaneous symmetry-breaking property of the shadow wave function. The final configurations display a face-centered-cubic structure grown preferentially by {111} planes, accompanied by stacking disorder.

I. INTRODUCTION

The microscopic description of phase transitions is a long-standing problem in many-body physics. Several works have been done on the freezing of classical systems by using computer simulations. Spontaneous nucleation of crystals in supercooled Lennard-Jones liquids have been found both with molecular dynamics (MD) and Monte Carlo (MC) studies.[1–3] The situation in the case of quantum systems is different. Path-integral Monte Carlo studies of quantum particles[4] at finite temperature show that at large enough density, when the simulation is started from an ordered configuration, the crystalline order remains present through the simulation. However, no attempts have been done to obtain crystallization in a simulation, starting from a liquidlike sample. In the standard variational theory of many-body systems at $T = 0$ K, the crystalline order is imposed by construction because each particle is localized around an assumed equilibrium position.[5,6] Therefore, such a ground-state trial wave function is not translationally invariant, and one cannot address the question of the nucleation of a crystal. On the contrary, this question can be addressed when the variational theory is based on a shadow wave function (SWF).[7,8]

From now on, we will consider only the case of Bose systems such as ^{4}He. In the SWF,[7,8] the correlations between particles in the ground state Ψ_0 arise in two ways, by explicit correlating factors of the Jastrow form and, implicitly, via a coupling of the positions of the particles to subsidiary variables, the shadows. In the standard representation of Ψ_0 only the explicit correlating factors are present. The SWF is translationally invariant but has two regimes, a fluid and a solid one, depending on the density and strength of the couplings. However, the solid phase was found in the system when starting either from an ordered configuration or a large crystalline seed imbedded in a liquidlike sample.[9] No report was given of crystalline order when the particles started from a disordered configuration.

Recently a new wave function of the shadow type and denoted as the local-density shadow wave function (LDSWF) has been proposed[10] to study liquid-solid coexistence and the interface of ^{4}He. This wave function is characterized by the fact that the shadow-shadow correlations are made explicitly dependent on the local density of the shadows $\hat{\rho}_i$, and this allows for using a unique set of variational parameters in the whole range of densities for the liquid and solid branch of the equation of state of atomic ^{4}He. Extensive numerical simulations have indeed shown that LDSWF can sustain, in a satisfactory manner, the liquid-solid coexistence. Also in this case part of the system started from an ordered configuration.

In this paper we study whether SWF and LDSWF are capable of providing spontaneous crystallization in superdense liquid ^{4}He, or whether crystalline order exists only when it is already present in the initial configuration. We present the results of Monte Carlo simulations, performed with 108 and 500 atoms, described by SWF and LDSWF, starting from an overdense liquid, without introducing any kind of seed, which shows spontaneous crystallization. The crystal we obtain shows a prevailing face center cubic (fcc) structure grown with the unit cell slightly tilted with respect to the cubic simulation box. The fcc structure presents distortions, due to incompatibilities with the periodic boundary conditions, and is accompanied by stacking faults in the piling of the {111}

0163-1829/95/52(10)/7564(8)/$06.00

planes.

The paper is organized as follows. The SWF and LDSWF are briefly reviewed in Sec. II. Section III discusses the simulation procedures and the estimators employed in studying the crystal growth. The results are presented in Sec. IV. Section V is devoted to conclusions.

II. SHADOW WAVE FUNCTIONS

The shadow wave function, introduced by Vitiello *et al.*,[7,9] is represented by the following convolution form:

$$\Psi(R) = \int dS\ K(R,S)\psi_s(S), \tag{1}$$

where $R = \vec{r}_1, \ldots, \vec{r}_N$ are the coordinates of the N atoms, $S = \vec{s}_1, \ldots, \vec{s}_N$ those of the auxiliary ("shadow") variables, and $\psi_s(S)$ is the shadow term in the wave function. The kernel $K(R,S)$ consists of a product of a function $\psi_r(R)$ correlating the particles and a function $\theta(R,S)$, which binds each particle $\vec{r}_i$ to the corresponding shadow $\vec{s}_i$, namely,

$$K(R,S) = \psi_r(R)\theta(R,S). \tag{2}$$

The functions $\psi_s(S)$, $\psi_r(R)$, and $\theta(R,S)$ are taken in the following form:

$$\psi_r(R) = \exp\left(-\frac{1}{2}\sum_{i<j} u_{pp}(r_{ij})\right), \tag{3}$$

$$\psi_s(S) = \exp\left(-\sum_{i<j} u_{ss}(s_{ij})\right), \tag{4}$$

$$\theta(R,S) = \prod_i e^{-C|\vec{r}_i - \vec{s}_i|^2}, \tag{5}$$

where u_{pp} and u_{ss} are variational functions and C is a variational parameter to be determined by minimization of the expectation value of the Hamiltonian. The simplest choice for u_{pp} and u_{ss} is of the so-called McMillan form, $u_{pp}(r) = (b_p/r)^5$ and $u_{ss}(s) = (b_s/s)^9$. The optimal values of C, b_p, and b_s are density dependent so that, even if the functional form is independent on density, the coupling parameters depend on the state of the system.

In the LDSWF,[10] the coupling parameters are assumed to depend on a local density operator $\hat{\rho}_i$ in such a way that a unique wave function describes the system over a wide range of densities comprehending both the liquid and the solid phase. The coupling parameter b_s is the one with the largest density dependence, and it has been shown[10] that a realistic parametrization of the pseudopotentials is

$$u_{pp}(r_{ij}) = \left(\frac{b_p}{r_{ij}}\right)^5, \tag{6}$$

$$u_{ss}(s_{ij}) = \left(\frac{b_s}{s_{ij}}\right)^9 = \left[\frac{b_0 + b_1(\hat{\rho}_i + \hat{\rho}_j)/2}{s_{ij}}\right]^9, \tag{7}$$

where b_p, b_0, b_1, and C are independent on density. The *local density operator* of shadows $\hat{\rho}_i$ appearing in Eq. (7) is represented by the following function:

$$\hat{\rho}_i = \frac{1}{A}\sum_l \nu_F(r_{il}) = \frac{1}{A}\sum_l \{1 + \exp[\mu(r_{il} - r_c)]\}^{-1}, \tag{8}$$

with A being a normalization constant. The parameters μ and r_c in the Fermi function $\nu_F(r)$ are determined following the criterion of reproducing the average density of shadows in homogeneous systems within a range including the first shell of neighbors in the liquid phase. The values $\mu = 3\sigma^{-1}$ and $r_c = 2.1\sigma$, with $\sigma = 2.556$ Å, have been found[10] to meet the above conditions. The other variational parameters were determined[10] by an overall minimization in the range of densities $0.365 < \rho\sigma^3 < 0.550$, with the result $b_p = 1.12\sigma$, $C = 4\sigma^{-2}$, $b_0 = 0.51\sigma$, and $b_1 = 1.91\sigma^4$. Clearly one recovers the SWF when $b_1 = 0$ and b_0 takes the value appropriate for the average density of the system.

Let us briefly report on simulations performed with the above LDSWF, starting from an ordered configuration. The evolution of the system strongly depends on the average density considered. When $\rho\sigma^3 \lesssim 0.44$, the system rapidly melts and a liquidlike $g(r)$ is found, both for particles and shadows. On the other hand, at larger densities ($\rho\sigma^3 \gtrsim 0.49$) the crystalline order is found to be stable. In fact, no diffusion is found in the system, but the shadows and the particles remain confined around their initial positions, as measured by Lindemann ratio and crystalline order parameters. Thus, we have a wave function that is translationally invariant with the crystalline order sustained by the correlations. The good value of the energy upperbound, compared with that of a standard Nosanow-Jastrow wave function, in which the crystalline order is explicitly introduced by one-body terms, proves that the LDSWF captures the basic physics of this quantum crystal. Stabilization of crystalline order in this wave function is due to the shadows, which behave rather like classical particles. This can be inferred, for instance, analyzing the pair distribution functions of the shadows that, in the case of the solid, have the typical sharply peaked structure found in analogous classical simulations. On the contrary the distribution of the atoms is much less structured, as can be seen in Fig. 1. The role of the core parameter b_s in $u_{ss}(s)$ is crucial in describing the phase of the system. This indicates that in the quantum case the excluded volume effects, which drive the crystallization, are not only due to the physical size of the particles but also to the excluded volume due to quantum fluctuations (the "correlation hole").

Similar considerations can be drawn by looking either at the crystalline order parameters or to the static structure factors $S_{\alpha\alpha}(\vec{k})$, given by

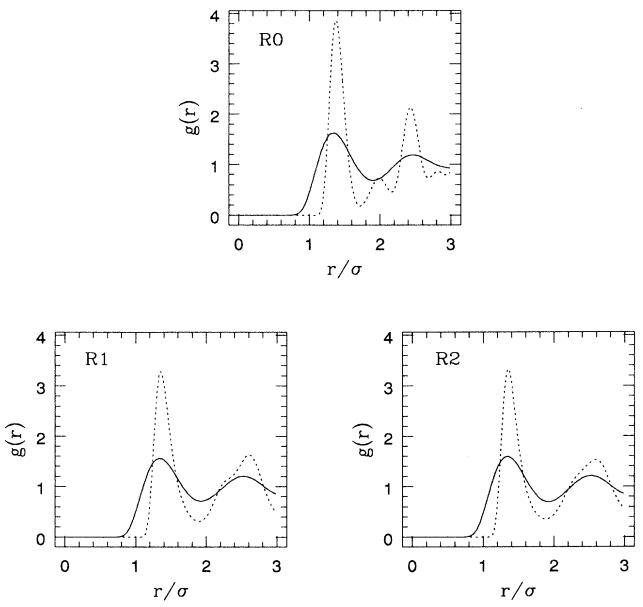

FIG. 1. Pair correlation functions for $R0$, $R1$, and $R2$ (see text): dotted line is g_{ss} and solid line is g_{pp}.

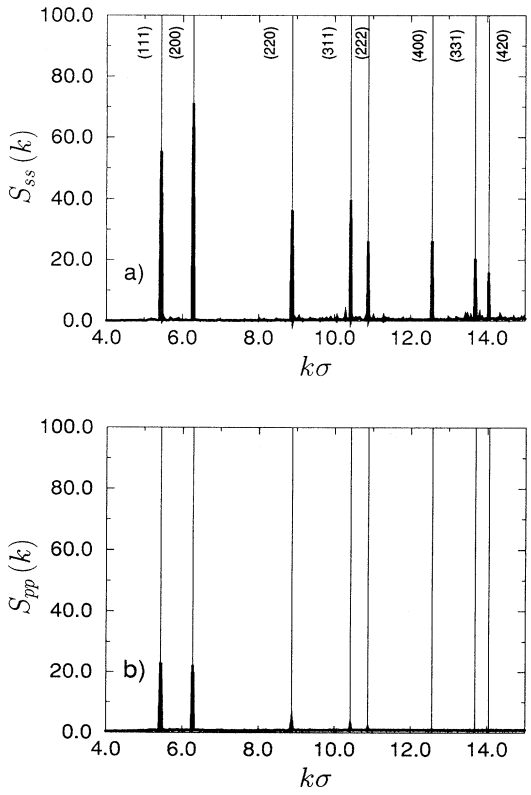

FIG. 2. Spherically averaged static structure factors measured on 160 configurations extracted from a simulation started from a perfect fcc crystal. (a) S_{ss} and (b) S_{pp}. The position of the reciprocal lattice vectors of a perfect fcc crystal indexed with respect to a cubic elementary cell, are also displayed.

$$S_{\alpha\alpha}(\vec{k}) = \frac{1}{N_\alpha}\langle \rho^\alpha_{-\vec{k}} \rho^\alpha_{\vec{k}} \rangle, \tag{9}$$

where the density fluctuation operator $\rho^\alpha_{\vec{k}}$ is given by

$$\rho^\alpha_{\vec{k}} \equiv \sum_{i=1,N_\alpha} e^{i\vec{k}\cdot\vec{x}^\alpha_i}, \tag{10}$$

where $\alpha = p, s$ for particles and shadows respectively, N_α is the number of particles of type α, and $\vec{x}^p_i = \vec{r}_i$ and $\vec{x}^s_i = \vec{s}_i$. The spherical average of $S_{ss}(\vec{k})$ presents sharp peaks in correspondence with the reciprocal lattice vectors of the crystalline structure, as can be seen from the case of a stable fcc structure, generated from an initial crystalline configuration at $\rho\sigma^3 = 0.5$, shown in Fig. 2. A comparison between $S_{ss}(\vec{k})$ and $S_{pp}(\vec{k})$ makes evident that shadows are much more localized than particles.

As previously discussed, in all the simulations with SWF and LDSWF, appearing up to now in the literature, in which a crystalline order has been found, either this order or at least a large seed of it was present in the initial configuration.

In the following section we answer the question whether or not SWF and LDSWF can spontaneously break the translational invariance. This can be verified first performing simulations starting from configurations, which are proper for the fluid phase, and then, after a rescaling of distances corresponding to a compression, measuring the crystalline order of the structure of the evolving system.

III. SIMULATION PROCEDURE

The calculations have been performed at the density value $\rho\sigma^3 = 0.5$, which is slightly above the melting density obtained from Green's-function Monte Carlo simulations[11] ($\rho\sigma^3 = 0.491$), and for which a stable solid phase has been found using LDSWF. The Monte Carlo simulation has been performed using the Metropolis algorithm, sequentially moving the real and the auxiliary degrees of freedom. A complete sweep over all the degrees of freedom is denoted as a Monte Carlo step (MCS). Details about the modification of the standard algorithm due to the presence of the shadows can be found in Ref. 9.

A first set of simulations has been performed with a cubic cell of side 6σ accommodating 108 particles, which exactly fits $3\times3\times3$ elementary conventional cubic cells of a fcc lattice. Periodic boundary conditions were imposed in all directions. A first run, hereafter considered as the reference run and denoted as $R0$, started from a perfect crystalline configuration, with $b_1 = 0$ and $b_0 = 1.465\sigma$, which is equivalent to using SWF. The same run has been repeated with 500 particles showing no appreciable differences with respect to $R0$. The configurations generated within this run have been used to calculate the structure factors displayed in Fig. 2. Two crystallization simulations were performed for 2×10^5 MCS's one with SWF and the other with LDSWF. Let us denote with $R1$ the SWF run ($b_0 = 1.4656\sigma$, $b_1 = 0$) and with $R2$ the

LDSWF run. In both cases we employed as a starting configuration that obtained from a simulation of a liquid at equilibrium density ($\rho\sigma^3 = 0.365$), after 5×10^4 MCS's, and rescaled to the density $\rho\sigma^3 = 0.5$.

Two other crystallization runs were performed with a larger number of particles ($N = 500$) in a cubic box and using LDSWF. The liquidlike initial configuration has been obtained as for the runs described before. Each run corresponds to an independent Markov chain of configurations, obtained by changing the seeds of the random-number generator and the step size of the proposed move both of particles and of shadows. They are denoted as runs $R3$ and $R4$. The center of mass of the system has been kept fixed; namely, all the coordinates are taken with respect to the center of mass of the system.

During the runs, spherical pair-correlation functions for particles $g_{pp}(r)$ and for shadows $g_{ss}(s)$ were estimated. Although these quantities are spherical averages, they still give important information on the crystalline structure of the system. Another important quantity that we have analyzed is the spherical average of the static structure factor $S_{\alpha\alpha}(\vec{k})$ given in Eq. (9). The numerical procedure used to compute $S_{\alpha\alpha}(\vec{k})$ is described in the Appendix.

IV. RESULTS

The occurrence and the nature of the crystallization has been studied by analyzing the pair-correlation function, the static structure factor, and by direct visualization of the configurations. Homogeneous nucleation of crystals has been found in all the simulations performed, although with slightly different characteristics.

Figure 1 shows the pair-correlation functions for both particles and shadows, evaluated on the last 10^5 MCS's of the simulations carried out with 108 atoms. The crystallization runs $R1$ and $R2$ differ from the reference run $R0$, particularly for the shadows, whose pair-correlation function g_{ss} has no apparent structure at $r \simeq 2\sigma$ and has peaks with a height that is $\sim 15\%$ smaller. In $R0$, $g_{ss}(r)$ displays all the proper peaks of a fcc lattice. As expected, the real particles are less localized than the shadows, although the height of the main peak (~ 1.6) indicates a localization, which is typical of a quantum solid. $R1$ and $R2$ do not show any appreciable difference, except for the occurrence of a structure in g_{ss} at $r \sim 2.3\sigma$, which is more pronounced in $R1$ than in $R2$. This confirms that, once a stable homogeneous phase is reached, SWF and LDSWF lead to the same description of the system.

Figure 3 displays the evolution of the crystallization during $R2$ for both particles and shadows. At the beginning of the run the system is still fluid; after 2×10^5 MCS's, the pair functions appear much more structured, as in the case of solids.

The pair-correlation functions obtained in the two independent runs with 500 atoms, and shown in Fig. 4, present features that clearly indicate the occurrence of a solidlike state as for the cases with 108 atoms. The two

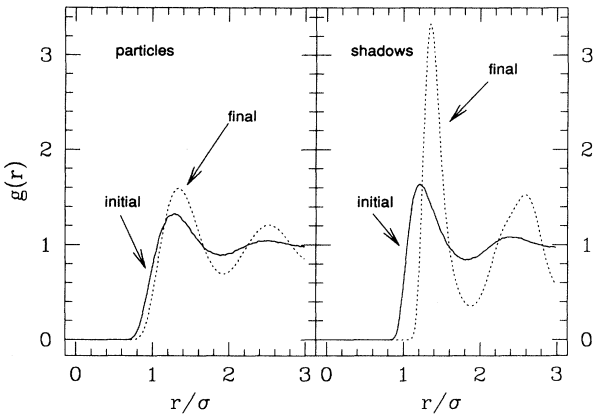

FIG. 3. Pair-correlation functions of particles and shadows for $R2$ (108 atoms with LDSWF) at the beginning of the run (solid line) and after 2×10^5 MCS's (dotted line).

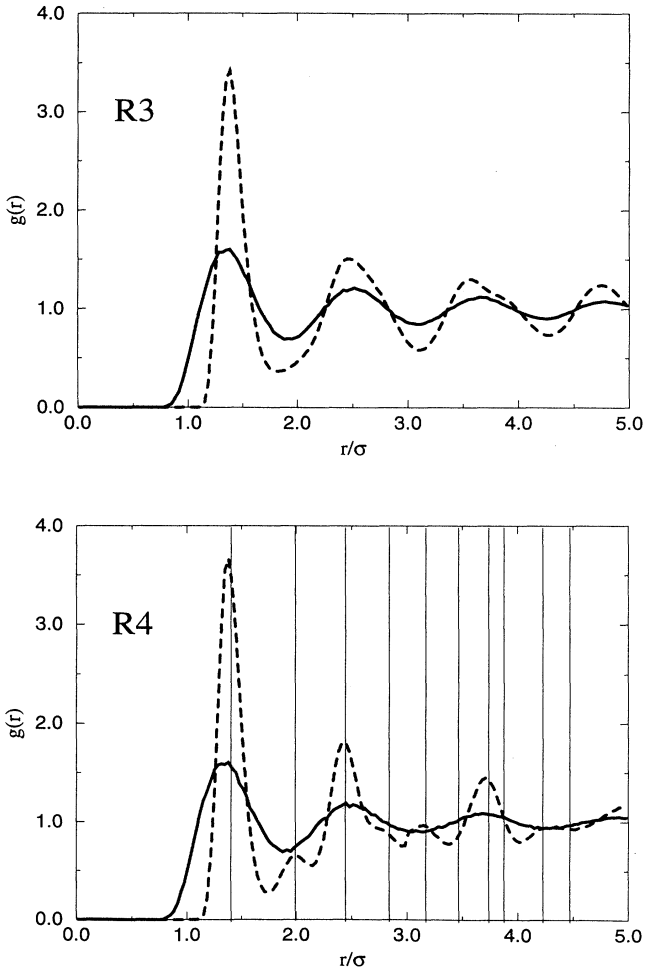

FIG. 4. Pair-correlation functions for N=500 particles with LDSWF for $R3$ and $R4$. Solid line is g_{pp} and dotted line is g_{ss}. The location of the fcc peaks are reported for convenience (their coordination numbers are, respectively, 12, 6, 24, 12, 24, 8, 48, 6, 36, 24). The first three peaks only are compatible with the hcp structure.

simulations have led to two different realizations of this state, although the resulting particle pair-correlations look very similar. During $R4$ the structural stability of the crystal was reached with fewer MCS's than during $R3$. In $R3$ the two main peaks of g_{ss} closely resemble those obtained with 108 atoms, with the second peak blurred out and without the presence of the second-neighbor peaks. This implies that if a structure is present the percentage of defects is quite high. In $R4$, $g(r)$ has much more structure and presents the gross features of a less defective crystal. The positions of the peaks are in good agreement with the distances of the neighbors in a fcc lattice. The missing ones, corresponding to the sixth and the eight neighbors indeed have a low coordination number. The peaks of $g(r)$ are in better correspondence with the fcc lattice than with the hexagonal close packed (hcp) one, but the spherically averaged $g(r)$ is not able to give clear evidence of which kind of order is present. In any case, the absence of diffusion proves that the system is in a solid phase.

Some more information can be obtained through the direct visualization of the configurations generated in the random walk. From the study of the correlation functions we have learned that the ordering properties are made more evident when looking at the shadow degrees of freedom rather than at the real particles. From the visualization of the configurations it is also possible to follow the pseudoevolution of the sample, observing the progressive growth of the crystalline order. There are several ways to study the configurations. The most suggestive consists in a three-dimensional (3D) visualization realizing a movie with the successive configurations. Another way consists of plotting the projection of the coordinates on a chosen plane (commonly one of the faces of the simulation box). The results reported below all refer to $R3$, which is the run showing a less evident ordering from the bare observation of the $g(r)$, so that it is the most interesting to analyze.

Figure 5 displays the projections of the coordinates of shadows in the x-z and in the x-y planes after about 8×10^4 MCS's. The positions of the shadows are far from being uniformly distributed, as in a fluid, and there is clear evidence of some crystalline ordering. This is particularly clear in the x-z projection, where we can distinguish three different regions, one on the top with planes oriented with an angle $\pi/4$ with respect to the axes, one in the middle where the shadows are already localized but the structure is not well defined yet, and one in the bottom, where the orientation of the planes looks to be parallel to the z axis. Also in the x-y projection it can be noticed that the orientation of the layers is not well defined, even if one can distinguish portions where the planes are ordered. This indicates that in the box the crystal growth does not start from a unique seed but rather from several seeds with different orientation and stacking. Thus, we can think of the evolution of our system as split in two different motions: one is the motion of the atoms around the instantaneous equilibrium position in the solid seeds, and the second one is the slower motion by which the crystal adjusts its symmetry and shape. This situation alters the generation of

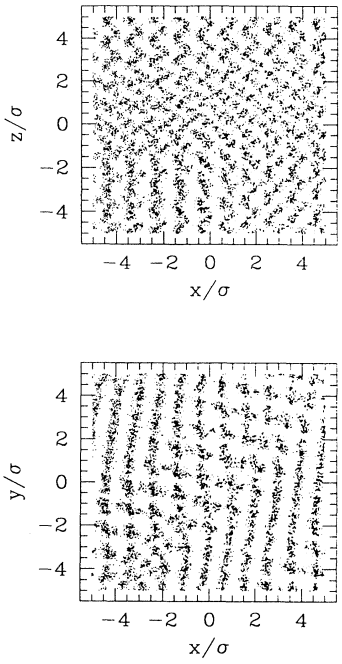

FIG. 5. Projection of 40 shadow configurations of $R3$ taken out from 1000 after $\sim 8\times10^4$ MCS's. Top is the x-z projection and bottom is the x-y projection.

the random walk, so that the acceptance rate of the trial moves for the shadows is gradually lowering during the simulation from 30% to 20%.

In the next stage of the simulation, we observe that one of the seeds prevails on the others. In Fig. 6 the projections on the faces of the simulation box of configu-

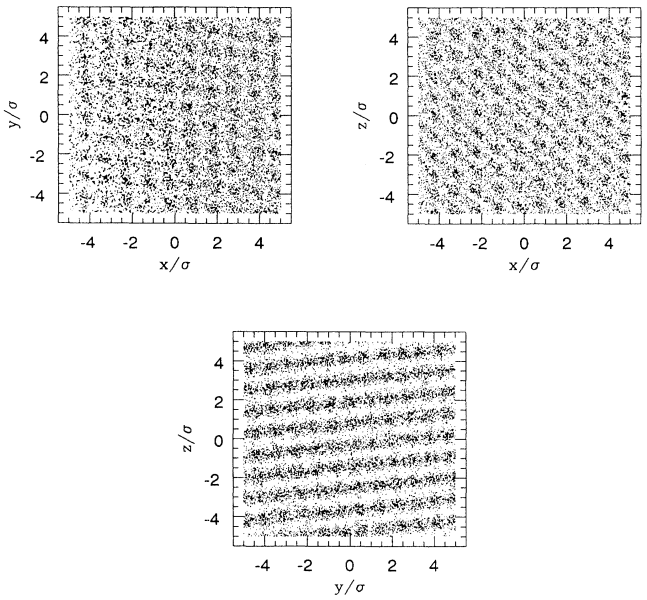

FIG. 6. Projections of the shadow configurations of $R3$ after 2×10^5 MCS's. Top left is the x-y projection; top right is the x-z projection; and bottom is the y-z projection.

rations generated after about 2×10^5 steps are shown. It can be seen that the situation is very different from that displayed in Fig. 5. In particular, the y-z projection presents a well-defined layering. The spacing among the layers is larger than $a/2$, as for $\{100\}$ planes of a perfect fcc lattice filling our simulation box, whereas it is very close to $a/\sqrt{3}$, typical of a $\{111\}$ stacking of fcc planes. Actually the spacing is slightly smaller than $a/\sqrt{3}$, indicating the presence of dishomogeneities in the crystal. Moreover, the crystalline planes are tilted with respect to the simulation box axes.

In Fig. 7 we show the projection of the shadow configurations onto the x-y plane after a rotation of an angle $\gamma = 6°36'$ around the x axis. After such a rotation all the planes clearly display an ordered situations, revealed by spots in correspondence to the lattice sites. The angle needed to perfectly align the crystalline planes to the axes of the simulation box ranges from $\sim 10°$ to $\sim 6°$.[12]

The structure displayed in Fig. 7 is very close to that typical of the close packing ordering. From figure (a) a sixfold coordination is very evident, and the rows along the x-y (rotated axis) bisector are almost perfect. Along the equivalent directions making an angle $\pm\pi/3$ with the bisector, one sees a clear ordering, but there is a modulation of the rows, which is almost sinusoidal. This is clearly due to the fact that a perfect closed packed plane is not compatible with the periodic boundary conditions of the cubic simulation box, unless the normal to the closed packed $\{111\}$ planes is parallel to the main diagonal of the simulation box. A possible explanation of why

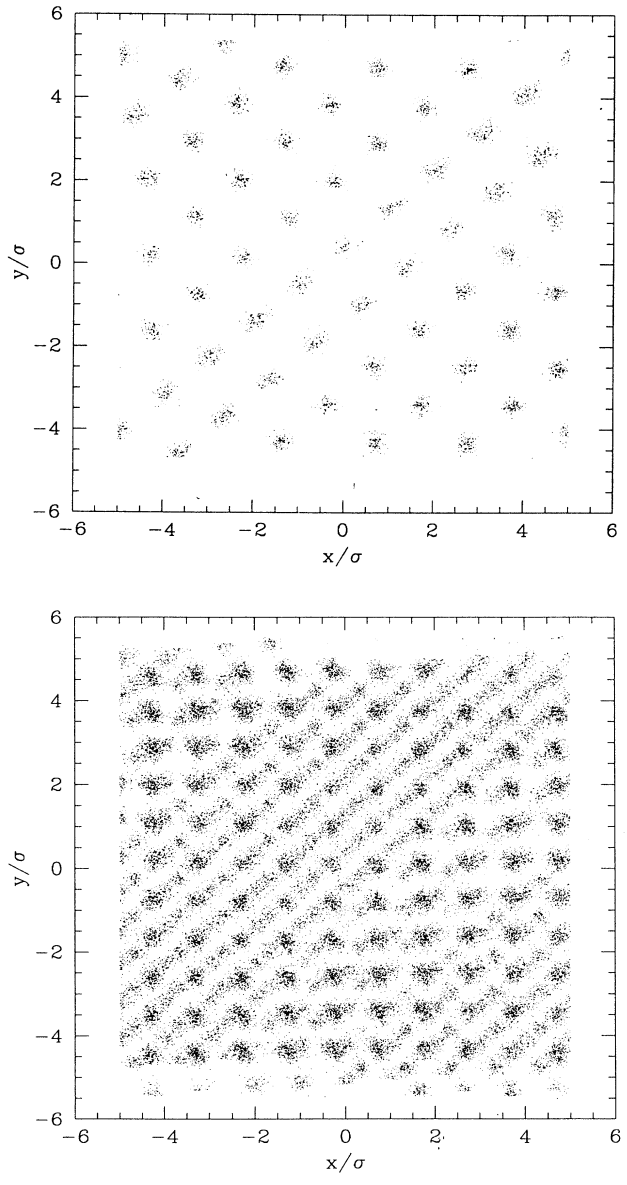

FIG. 7. x-y projection of the shadow configurations after 2×10^5 MCS's of $R3$ and after a rotation of $6°36'$ around the x axis: (a) $2.5\sigma \leq z \leq 3.5\sigma$ (single plane) and (b) $0 \leq z \leq 6\sigma$.

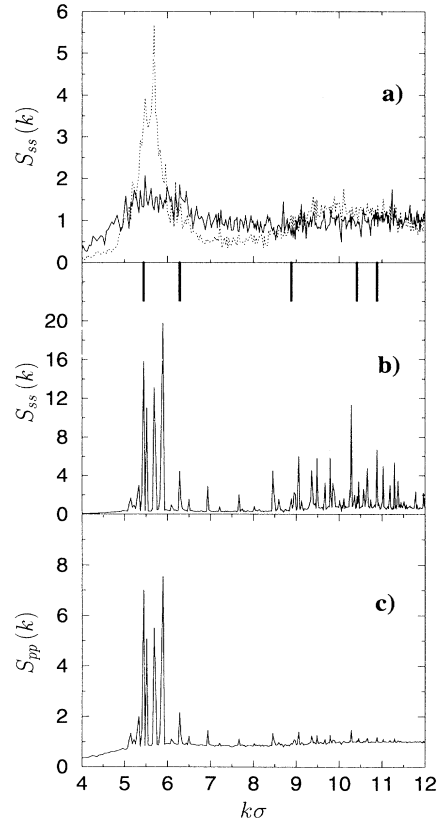

FIG. 8. Spherically averaged static structure factors for shadows and particles in $R3$: (a) $S_{ss}(k)$ at the beginning of the run (solid line), and after 1.2×10^5 MCS's (dotted lined), obtained from one configuration; (b) $S_{ss}(k)$ after 3×10^5 MCS's, obtained from 160 configurations out of 8000 MCS's; the thick lines in the upper part correspond to the positions of the reciprocal lattice vectors for a fcc structure of lattice constant $a = 2\sigma$; and (c) $S_{pp}(k)$ after 3×10^5 MCS's, obtained from 160 configurations out of 8000 MCS's.

TABLE I. Variational energies and potential and kinetic energies per particle in the crystallization runs.

Run	Ψ	Initial conf.	ϵ (K)	$E_{\rm kin}$ (K)/N	$E_{\rm pot}$ (K)/N	MCS's
$R0$	SWF	solid	-4.82 ± 0.01	26.47 ± 0.03	-31.30 ± 0.03	5×10^4
$R3$	LDSWF	fluid	-4.33 ± 0.01	26.32 ± 0.03	-30.65 ± 0.01	3×10^5
$R4$	LDSWF	fluid	-4.23 ± 0.01	26.30 ± 0.03	-30.54 ± 0.02	1×10^5

the system crystallizes with a tilting angle γ of the closed packed planes, which is smaller than the value required in order to have no distortion, is the following. The area of a closed packed plane inside the box has the largest value when the normal to this plane is along the diagonal of the box, and diminishes for decreasing values of γ. On the other hand, ordering is favored if the length over which the periodic boundary conditions are imposed is small. Therefore, we can understand the observed small value of γ as due to a competition between this ordering effect, which pushes γ to zero, and the associated distortions of the lattice, which grow as $\gamma \to 0$.

It is also interesting to look at the stacking of successive planes. Overlapping the configurations of the single planes, as done in Fig. 7(b), it is possible to distinguish regions where the stacking is threefold (typical of the fcc lattice), and regions where there is a twofold stacking (typical of the hcp lattice).

A further evidence for the crystallization of the sample, as well as the indication for the occurrence of a combination of a prevailing fcc lattice, comes from the structure factors. Figure 8 displays the evolution of $S_{ss}(k)$ of $R3$; starting from the initial compressed liquidlike configuration [Fig. 8(a), solid line] the structure factor, at first grows, showing still a metastable liquid phase after 1.2×10^5 MCS's [Fig. 8(a), dotted line]; then at about

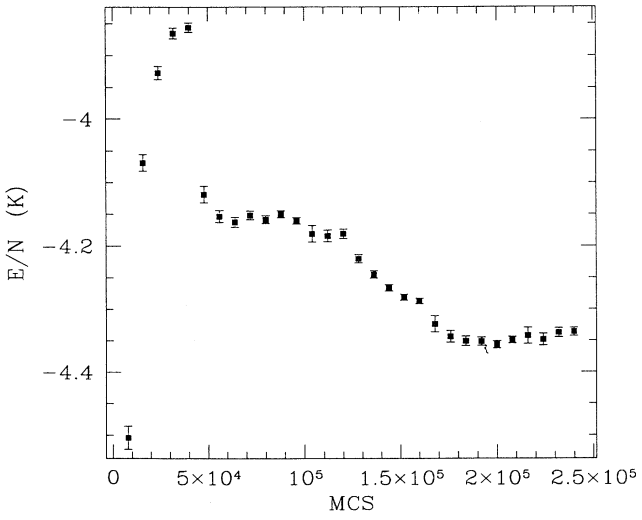

FIG. 9. Average value of the energy on blocks of 8000 MCS's, for the first 2.4×10^5 MCS's in $R3$.

4×10^4 MCS's crystalline peaks appear and grow out of the liquidlike pattern, and finally it becomes stable after 1.2×10^5 MCS's. The final result, obtained after 3×10^5MCS's, on 160 configurations out of 8000, is shown in Fig. 8(b), where the thick marks on the upper part signal the positions of the fcc reciprocal lattice vectors. One can see the growth of a series of sharp, well resolved peaks, that clearly indicate the formation of a crystalline structure. Some of these peaks, as shown in the figure, can be labeled as the reflection of a fcc structure of lattice parameter $a = 2.\sigma$. The remaining peaks cannot be easily assigned without doing further specific analyses, which, however, go beyond the scopes of the present work. They probably correspond to the presence of stacking disorder in a fcc structure.[13,14] Figure 8(c) displays the structure factor $S_{pp}(k)$ of $R3$. A comparison of Figs. 8(b) and 8(c) confirms the feature that the particles are less localized than the shadows. The heights of the peaks of $S_{pp}(k)$ are quenched with respect to the corresponding ones of $S_{ss}(k)$ by about 60%.

Putting together all the information from pair-correlation functions, structure factors, and direct visualization of the configurations, we may conclude that the system crystallizes with a prevailing fcc structure, which is distorted because the direction of the crystal growth is such that a perfect fcc structure is not compatible with the periodic boundary conditions. In addition, the fcc structure is accompanied by stacking faults of the {111} fcc layers.

The expectation value of the energy obtained, respectively, in runs $R0$, $R3$, and $R4$, together with the potential and the kinetic energy, are reported in Table I. The interatomic potential considered is the Aziz HFDHE2 potential.[15] The main feature that can be observed is that in all the crystallization runs there is a difference of $\sim 0.5 - 0.6$ K with the energy upperlimit of the reference case. This is due to the defects of the grown crystal. From Figs. 6 and 7 one can see that the lattice constant a varies locally from $\sim 1.95\sigma$ to $\sim 2.\sigma$, and, correspondingly, the local density varies from $\sim 0.55\sigma^{-3}$ to $\sim 0.5\sigma^{-3}$. As a consequence, the energy per particle may range from ~ -3.7 K to ~ -4.8 K. In Fig. 9 the evolution of the expectation value of the energy in the course of a typical run is displayed. It starts from a quite low value, which gradually increases. At this stage of the simulation one has solid seeds embedded in the fluid. The cost of the interface increases the energy of the system. After this barrier is overcome, the variational energy begins to lower again, soon reaching a nearly constant value. Presumably, much longer runs are needed to recover the lower equilibrium value of the energy.

V. CONCLUSIONS

In this paper we have presented the results obtained with Variational Monte Carlo calculations on atomic ^{4}He with shadow wave functions at a density well above the melting density, starting from initial configurations of a superdense fluid. A stable crystalline phase has been reached in all the simulations, proving that SWF and LDSWF provide a true stable ordered phase at high enough densities. The results obtained strongly support that the growing process is favored for the {111} planes, resulting in the fact that the system prefers to tilt the planes and to adjust them to the cubic box rather than growing nonclose packed planes. The resulting crystal has a prevailing fcc structure accompanied by stacking disorder. We expect that similar results are also obtained if the shadow-shadow correlation pseudopotential is taken for the rescaled Aziz form,[16] which is known to provide better variational results for the equation of state. Work in this direction is in progress.

ACKNOWLEDGMENTS

We would like to thank S. A. Vitiello, M. H. Kalos, and E. Tosatti for enlightening discussions on the subject of this paper. This work was partially supported by MURST and by INFM.

APPENDIX A

The structure factors given in Eq. (9) have been computed following the procedure of Ref. 1, which we briefly outline in this appendix.

Inserting Eq. (10) into Eq. (9), one obtains the following two equivalent expressions:

$$S_{\alpha\alpha}(\vec{k}) = \frac{1}{N_\alpha}\left\langle \sum_{i,j}^{N_\alpha} \exp(-i\vec{k}\cdot\vec{r}_{ij}) \right\rangle \tag{A1}$$

and

$$S_{\alpha\alpha}(\vec{k}) = \frac{1}{N_\alpha}\left\langle \left| \sum_{i}^{N_\alpha} \exp(-i\vec{k}\cdot\vec{r}_i) \right|^2 \right\rangle. \tag{A2}$$

The second expression is more convenient to use in numerical simulations because it scales more favorably with the number of particles. We have evaluated the expression (A2) on the set of configurations obtained in the various runs for $\vec{K}$ values discretized on a cubic grid, compatible with the periodic boundary conditions, given by

$$\vec{K} = K_{\min}(n_1\hat{x} + n_2\hat{y} + n_3\hat{z}), \tag{A3}$$

with n_1,n_2,n_3 integers, and the minimum length $K_{\min} = 2\pi/L$ is related to the largest wavelength fluctuation compatible with the simulation box size. The factor $\exp(i\vec{K}_{\min}\cdot\vec{r}_i)$ is computed only once for each particle position, and the values corresponding to other values of $\vec{K}$ can be obtained by simple multiplications. The angle average is performed by averaging $S_{\alpha\alpha}(\vec{K})$ for those values of $\vec{K}$ in the cubic grid, having the same length, and different orientation.

* Present address: Laboratorio di Fisica Computazionale, Dipartimento di Fisica, Università di Trento, I-38050 Povo, Trento, Italy.

[1] M.J. Mandell, J.P. McTague, and A. Rahman, J. Chem. Phys. **64**, 3699 (1976).
[2] J.D. Honeycutt and H.C. Andersen, Chem. Phys. Lett. **108**, 535 (1984); J. Chem. Phys. **90**, 1585 (1986), and references therein.
[3] D. Frenkel, Annu. Rev. Phys. Chem. **31**, 491 (1980).
[4] E.L. Pollock and D. M. Ceperley, Phys. Rev. B **30**, 2555, (1984); K.J. Runge and G.V. Chester, Phys. Rev. B **38**,135 (1988).
[5] D.M. Ceperley and M.H. Kalos, in *Monte Carlo Methods in Statistical Physics*, Topics in Current Physics Vol. 7, edited by K. Binder (Springer, Berlin, 1979).
[6] K.E. Schmidt and D.M. Ceperley, in *Monte Carlo Methods in Condensed Matter Physics*, Topics in Applied Physics Vol. 71, edited by K. Binder (Springer, Berlin, 1992).
[7] S.A. Vitiello, K. Runge, and M.H. Kalos, Phys. Rev. Lett. **60**, 1970 (1988).
[8] L. Reatto and G. L. Masserini, Phys. Rev. B **38**, 4516 (1988).
[9] S.A. Vitiello, K. Runge, G.V. Chester, and M.H. Kalos, Phys. Rev. B **42**, 228 (1990).
[10] F. Pederiva, A. Ferrante, S. Fantoni, and L. Reatto, Phys. Rev. Lett. **72**, 2589 (1994); Physica B **194-196**, 967 (1994).
[11] M.H. Kalos, M.A. Lee, P.A. Whitlock, and G.V. Chester Phys. Rev. B **24**, 115 (1981).
[12] Further simulations performed with $N = 500$ particles and changing the random number sequence show that this behavior is always present. Moreover, the orientation of the order of growth is found to be equally distributed with respect to the ⟨100⟩, ⟨010⟩, and ⟨001⟩ directions in the various samples.
[13] S. Hendrics and E. Teller, J. Chem. Phys. **10**, 147 (1942); A.C. Wilson, Proc. R. Soc. London, Ser. A **180**, 277 (1942).
[14] L. H. Schwartz and J.B. Cohen, in *Diffraction from Materials* (Academic, New York, 1977), pp. 393–403.
[15] R.A. Aziz, V.P.S. Nain, J.S. Carley, W.L. Taylor, and G.T. McConville, J. Chem. Phys. **70**, 4330 (1979).
[16] T. McFarland, S.A. Vitiello, and L. Reatto, J. Low Temp. Phys. **89**, 433 (1992); T. McFarland, S.A. Vitiello, L. Reatto, G.V. Chester, and M.H. Kalos, Phys. Rev. B **50**, 13 577 (1994).